Journal of Applied Polymer Science

Solvent-induced crystallization of a polycarbonate surface and texture copying by polydimethylsiloxane for improved surface hydrophobicity

B. S. Yilbas,[1] H. Ali,[2] N. Al-Aqeeli,[2] M. Khaled,[3] N. Abu-Dheir,[2] K. K. Varanasi[4]

[1]Mechanical Engineering Department and Excellence in Renewable Energy, King Fahd University of Petroleum and Minerals, Dhahran 31261, Saudi Arabia

[2]Mechanical Engineering Department, King Fahd University of Petroleum and Minerals, Dhahran 31261, Saudi Arabia

[3]Chemistry Department, King Fahd University of Petroleum and Minerals, Dhahran 31261, Saudi Arabia

[4]Mechanical Engineering, Massachusetts Institute of Technology, Boston, Massachusetts

Correspondence to: B. S. Yilbas (E-mail: bsyilbas@kfupm.edu.sa)

ABSTRACT: The influence of the immersion period on the crystallization of polycarbonate (PC) was investigated, and the resulting texture configurations of the crystal structures were reconstructed with polydimethylsiloxane (PDMS). Analytical tools, including optical microscopy, scanning electron microscopy, atomic force microscopy, X-ray diffraction, the sessile drop technique, Fourier transform infrared spectroscopy, microtribometry, and ultraviolet–visible spectrophotometry, were used to characterize crystallized PC and PDMS surfaces. We found that the crystallized PC surface possessed microsize/nanosize spherulites, voids, and fibrils, and the increasing immersion period increased the texture height and spherulite concentration at the surface. The residual stress in the crystallized PC wafer was compressive, and it was on the order of −30 MPa. The friction coefficient of the crystallized PC surface remained lower than that of the as-received PC wafer, and the increase in the immersion period lowered the friction coefficient. The crystallized PC surface demonstrated superhydrophobic characteristics, and the maximum contact angle occurred with 6 min of immersion. The PDMS exactly reconstructed the texture of the crystallized PC surface, except those of the nanofibrils and subnanofibrils. The droplet contact angle attained a higher values for the PDMS replicated surfaces than for those corresponding to the crystallized PC wafer. © 2016 Wiley Periodicals, Inc. J. Appl. Polym. Sci. **2016**, *133*, 43467.

KEYWORDS: crystallization; hydrophilic polymers; polycarbonates

Received 28 October 2015; accepted 25 January 2016
DOI: 10.1002/app.43467

INTRODUCTION

Creating self-cleaning surfaces is one of the current challenges for achieving self-sustainable, clean surfaces under harsh environmental conditions. Self-cleaning surfaces, such as lotus leaves, rice leaves, red rose petals, and fish scales,[1–5] are present in nature, and mimicking nature enables us to fulfill the desire of achieving self-cleaning surfaces. Hydrophobicity is one of the key properties in these surfaces, and it is required for the self-cleaning of surfaces.[6] The characteristics of surface hydrophobicity depend on the surface texture and surface free energy; in this case, a surface texture composed of micropillars/nanopillars with a low surface energy is desirable.[6] Several methods have been reported and strategies have been introduced to improve the surface hydrophobicity.[7–16] In general, these methods are associated with multistep procedures and mostly involve harsh conditions, specialized reagents, and high costs. Some of these methods include phase separation,[7] electrochemical deposition,[8] plasma treatment,[12] sol–gel processing,[13] electrospinning,[14] laser texturing,[15] and solution immersion.[16] During these processes, the free energy of the surfaces is modified via changes in the compositions through chemical and physical reactions. On the other hand, surface texturing has many challenges in terms of cost, processing time, equipment, and skilled manpower requirements. In general, a cost-effective, one-step process of surface texturing is in demand and requires extensive research and development in the area of surface engineering. On the other hand, polycarbonate (PC) wafers can replace glasses for protection from environmental hazardous in domestic applications and industry because of its superior properties, including its high impact resistance, good optical transmission in the visible range, low modulus of elasticity, and good machinability.[17–20] The crystallization of PC surfaces under a controlled environment generates surface textures composed of microstructures/nanostructures; this significantly improves the surface hydrophobicity.[15] Because of the molecular distortion and optical scattering of the crystallized surface, the optical transmission

of the textured surface decreases significantly.[15] This limits the application of the textured surface when the transmittance of the visible spectrum of light is required. However, polydimethylsiloxane (PDMS) is a widely used silicon-based organic polymer that is optically clear, inert, nontoxic, and nonflammable. The liquid form of PDMS has superior rheological properties, and it offers one an alternative for copying and reproducing textured wafer surfaces. Although the reconstruction of the surface texture with PDMS has been reported in previous studies,[21] the process involved and the characteristics of the reproduced surface require further investigation to achieve an exact copy of the involved texture, particularly for surfaces with complicated geometric configurations, such as in the acetone-induced crystallization of the PC surface.[22]

Considerable research studies have been carried out to examine the hydrophobic characteristics of PC surfaces. The modification of PC with hydrophilic/hydrophobic coatings for the fabrication of microdevices was studied by Jang *et al.*[23] They demonstrated that with the hydrophilic treatment of PC, microchannels could be produced; these were resistant to organic solvents. The dual effects of self-cleaning polymeric materials incorporating the hydrophobic and photoactive approaches were investigated by Soliveri *et al.*[24] They showed that multilayer polymeric/TiO_2 composites with double self-cleaning properties, which implied both photooxidation and antisticking, could be produced. The surface modification of PC with a UV laser was realized by Jiang *et al.*[25] They indicated that a porous microstructure with periodical V-type grooves was generated; this improved the surface hydrophobicity. The influence of crystallization on the hydrophobic characteristics of PC was examined by Zhou *et al.*[26] Their findings revealed that the surface hydrophobicity of PC was enhanced when the material surface was crystallized via the solvent-induced method. The microtexturing of PC surfaces for improved hydrophobicity was investigated by Bhagat and Gupta.[27] They showed that that the PC surface did not undergo any chemical change during thermal replication and further implied that the resulting superhydrophobic behavior was solely due to the physical modification of the surface. Hydrophilization and hydrophobic recovery in polymers obtained by the casting of polymer solutions on the water surface were studied by Bormashenko *et al.*[28] The findings revealed that, after removal from the water surface, the polymer films had their hydrophobicity restored with time and the characteristic time of hydrophobic recovery was on the order of magnitude of hours. The modification of the PC surface by hierarchical microstructuring/nanostructuring was examined by Saarikoski *et al.*[29] They demonstrated that the water contact angle increased considerably with a hierarchical microstructure/nanostructure. In addition, the transmittance of PC increased and the surface reflection decreased with nanopatterning. The hydrophobic surfaces of polyacrylate–PDMS copolymers for anti-icing were examined by Yu *et al.*[30] They indicated that microphase separation appeared in all of the copolymers; this was associated with the aggregation of PDMS chains on the top of the polymer surfaces. This weakened the interaction between the polymer surface and water, mainly hydrogen bonding; this resulted in decreased water contact angle hysteresis.

The influence of the average surface roughness on the formation of superhydrophobic polymer surfaces through spin coating with hydrophobic fumed silica was investigated by Soz *et al.*[31] They indicated that the chemical structure and nature of the polymeric substrate played a significant role in the topography and average roughness of the silica-coated surfaces. The processing of hydrophobic nanopillar polymer surfaces with a nanoporous alumina template was examined by Huang *et al.*[10] They demonstrated that the contact angles of the molded plastic thin film with the nanopillars exceeded those of the films without the nanopillar surfaces. In addition, the hydrophilic properties of molded plastic thin film without nanopillars changed to hydrophobic properties through the formation of nanopillars at the surface. Mechanical-strain-induced wetting transitions between anisotropic and isotropic on PDMS films were examined by Goel *et al.*[32] They showed that on wrinkled PDMS films, the liquid droplet exhibited anisotropic wetting; this resulted in a higher contact angle in the direction perpendicular to the wrinkle axis. The influence of the wettability and surface roughness of the PDMS films treated by coupled oxygen plasma was studied by Juarez-Moreno *et al.*[33] Their findings revealed that enhancements in the adhesion strength were attributed to the increased mechanical interlocking driven by increased roughness and the formation of hydrophilic functional groups. Thermally stable PDMS derived for superhydrophobic surfaces was investigated by Liu *et al.*[34] They showed that the superhydrophobicity of the surfaces could thermally recover after oil contamination because of their high thermal stability below 500 °C. The evaluation of the polymer hydrophobic recovery behavior after H_2O plasma processing was studied by Tompkins and Fisher.[35] They indicated that high-density polyethylene and PC exhibited minimal hydrophobic recovery because of plasma-induced crosslinking and intrinsic thermal stability, respectively. Patterned polymer surfaces with wetting contrasts prepared by polydopamine modification was investigated by Zhang *et al.*[36] They demonstrated that when a hierarchical structured film was used, the uncoated and coated regions had similar static wettabilities but different dynamic wetting behaviors. A study on the surface modification of a group of polymers with a low-temperature cascade arc torch was carried out by Gilliam and Yu.[37] They showed that the surface oligomer formation was due to alkoxy degradation reactions and chain scission from overexposure to high-energy species.

The surface texturing of PC wafers for improved hydrophobicity was carried out previously[15,22]; however, the optical transmittance of the textured surfaces remained low. This limited the textured surfaces for practical applications, such as solar energy harvesting. One of the solutions to the optical transmittance problem is to replicate the textured surface with PDMS because PDMS has a high transmittance in the visible spectrum. Although PDMS has superior rheological properties, the replication of complex textures such as those formed on the crystallized PC surface is challenging. Consequently, in this study, the surface texturing of PC wafers through acetone-induced crystallization and the replication of textured surfaces with PDMS were investigated. The influence of the crystallization periods on the surface texture and topology of the replicated surfaces is

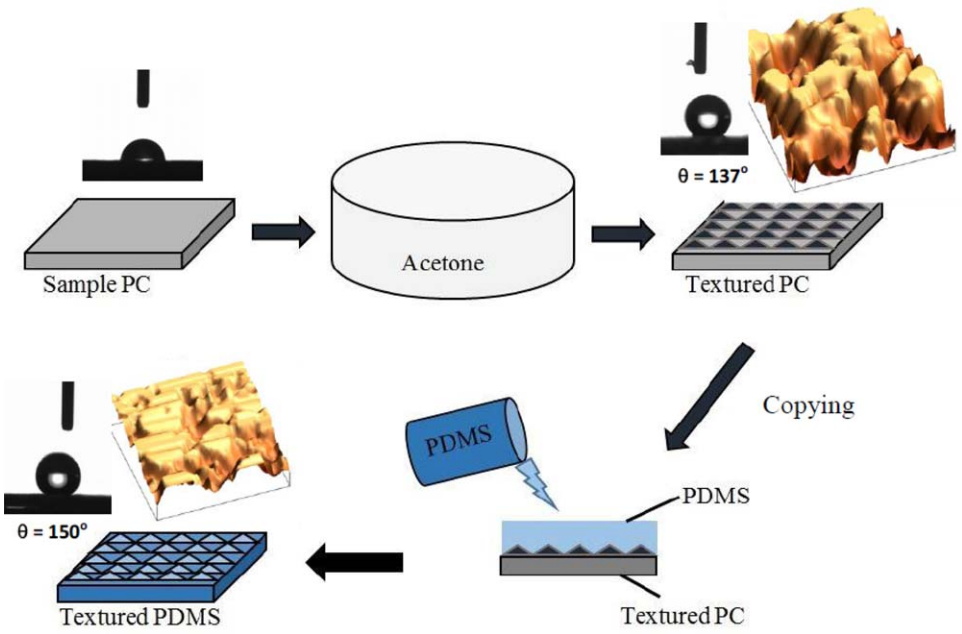

Figure 1. Schematic view of the crystallization of PC and the copying of the crystallized surface with PDMS. θ is the contact angle. [Color figure can be viewed in the online issue, which is available at wileyonlinelibrary.com.]

presented. The optical, morphological, and hydrophobic characteristics of the textured and replicated surfaces were examined with the analytical tools, including optical microscopy, scanning electron microscopy (SEM), atomic force microscopy (AFM), X-ray diffraction (XRD), and Fourier transform infrared (FTIR) spectroscopy. The tribological properties of the resulting surfaces were analyzed through scratch tests. The hydrophobicities of the surfaces were also assessed by the sessile drop measurement technique.

EXPERIMENTAL

PC wafers with 3-mm thicknesses were used as workpieces. The PC wafer was derived from A 4-Phenyl-3-Butenoic Acid (PBA) (*p*-hydroxyphenyl) and had excellent optical clarity with a high toughness. After ultrasonic cleaning, the PC wafers were immersed in liquid acetone for 2, 4, 6, 8, and 10 min. To select the immersion durations for the crystallization of PC wafers, several tests were conducted. The immersion durations resulting in crystal structures toward the formation of a surface texture for hydrophobic behavior were selected. Liquid PDMS, which belongs to a group of polymeric organosilicon compounds, was used to replicate the crystallized PC wafer surface. Liquid PDMS was deposited and left on the crystallized PC surface for over 18 h for curing purposes. The solidified PDMS was then removed from the crystallized PC surface after the curing period. Figure 1 shows the schematic view of the crystallization of the PC wafers and the copying of the resulting textured surface by PDMS.

The material and surface characterizations of the crystallized and copied PDMS surfaces were carried out with XRD and SEM, respectively. A JEOL 6460 electron microscope was used for SEM examinations, and a Bruker D8 Advanced instrument with Cu Kα radiation was used for XRD analysis. Typical settings for XRD were 40 kV and 30 mA, and the scanning angle ranged from 20 to 80°. An AFM/SPM microscope from Agilent in contact mode was used to analyze the surface texture. The tip was made of silicon nitride probes with tip radius of 20–60 nm ($r = 20$–60 nm) and manufacturer-specified force constant of 0.12 N/m.

The surface microhardness was measured with digital microhardness tester (MP-100TC). The standard test method was used for the hardness measurements (ASTM C1327-99). To determine the repeatability of the hardness data, the measurements were repeated three times at each location.

FTIR spectroscopy was carried out with a Nicolet Nexus 670 FTIR spectrometer. A Kyowa goniometer (model DM 501) was used to conduct sessile drop tests for the measurement of the droplet contact angle. Deionized water was used in the sessile drop experiments, and the droplet volume was controlled with an automatic dispensing system. The images of droplets were taken after 1 s of deposition of the water droplet on the surface. Ultraviolet–visible (UV–vis) spectroscopy (UV-2600, Shimadzu) was used to measure the transmittance of the workpieces.

The curvature method was used to determine the residual stress (σ) in crystallized PC wafers. The final deflection of curvature (Δx) of the crystallized wafers was recorded with the optical imaging technique. The equation relating Δx to the curvature (κ) can be written from the geometric relation[38]:

$$\kappa = \frac{1}{R} = \frac{L_{\text{arc}}}{\cos^{-1}\left(1 - \frac{\Delta x}{R}\right)} \quad (1)$$

where R is the curvature radius and L_{arc} is the arc length of the specimen. The Stony equation[38] provides the relationship between σ and the measured curvature:[38]

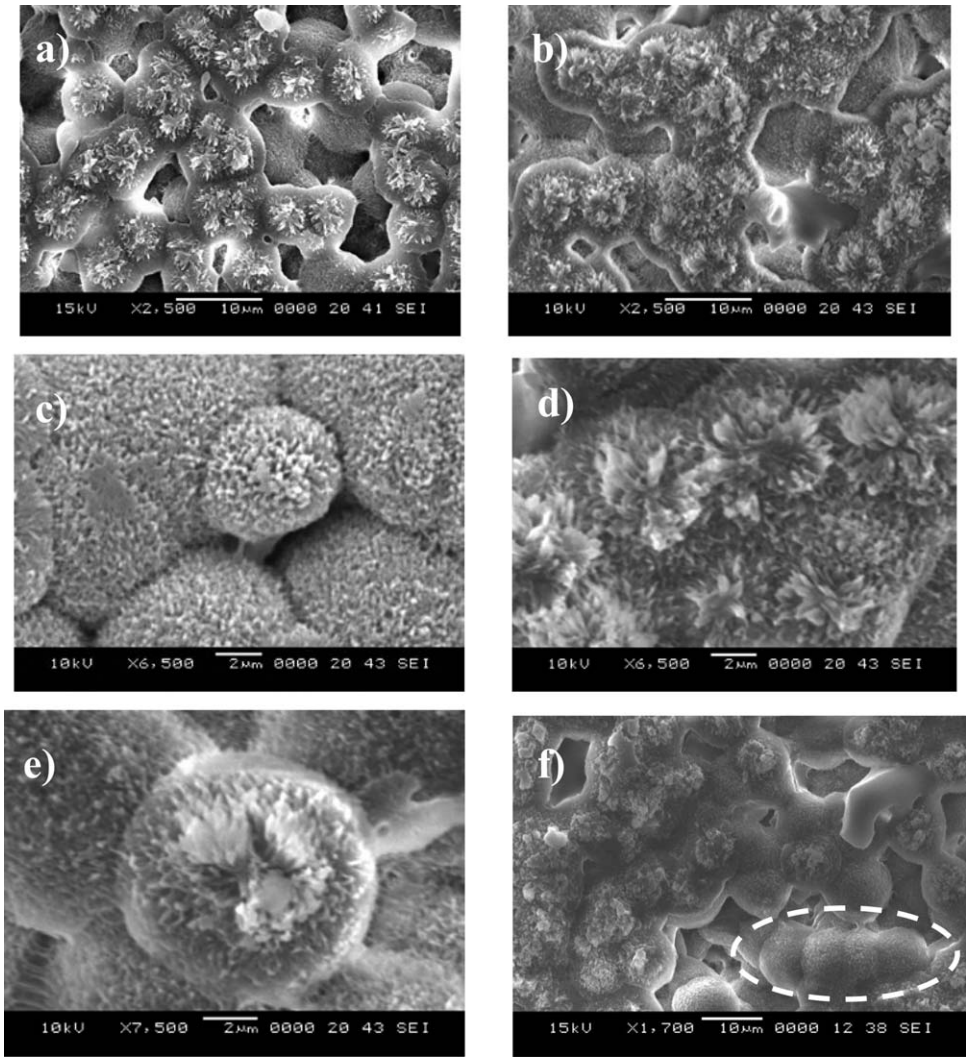

Figure 2. SEM micrographs of the crystallized PC surfaces: (a) PC surface after 2 min of immersion, (b) PC surface after 6 min of immersion, (c) initiation of fibrils after 2 min of immersion, (d) fibrils covering the almost spherulite surface, (e) fibrils formed at the spherulite surface, and (f) radial growth of the spherulites.

$$\sigma = \frac{\kappa E_s t_s^2}{6(1-\upsilon_s)t_c} \tag{2}$$

where E_s is the elastic modulus (2.4 GPa), t_s is the workpiece thickness, υ_s is Poisson's ratio (0.37) of the PC glass, and t_c is the crystallized layer thickness.

The scratch hardness (H_s) values of the crystallized PC and copied PDMS surfaces were evaluated in line with the ASTM D 7027-05. Consequently, the linear microscratch tester (MCTX-S/N: 01-04300) was used, and H_s data were recorded. In this case, the scratch tester was set at a contact load of 0.03 N and an end load of 5 N. The scanning speed was set at 5 mm/min with a loading rate of 5 N/s; this gave rise to a total scratch length of 5 mm. According to ASTM D 7027-05, H_s could be written as follows:[39]

$$H_s = \frac{4qP}{\pi w^2} \tag{3}$$

where P is the normal load used in the scratch tests (N), w is the scratch width (mm), and q is the dimensionless parameter ($q = 2$), which depends on the extent of elastic recovery of the polymer during scratching. In this case, full elastic recovery implies a value of $q = 1$, whereas no recovery implies a value of $q = 2$.

RESULTS AND DISCUSSION

The morphological and tribological characteristics of crystallized PC surfaces and copied textures on PDMS were examined with analytical tools.

Figure 2 shows SEM images of the crystallized PC surfaces with various immersion periods in liquid acetone. In general, the surfaces were composed of microstructures/nanostructures consisting of spherulites, pores, cavities, and nanosize fibrils [Figure 2(a,b)]. The spherulite size remains small for the case of a short immersion duration [2 min; Figure 2(a)], and the spherulites covered a large area at the surface for 6 min of immersion [Figure 2(b)]. In addition, the scattering of a small number of spherulites was observed at the surface [Figure 2(a)]. As the immersion time progressed ($\geq$2 min), the size of the spherulites

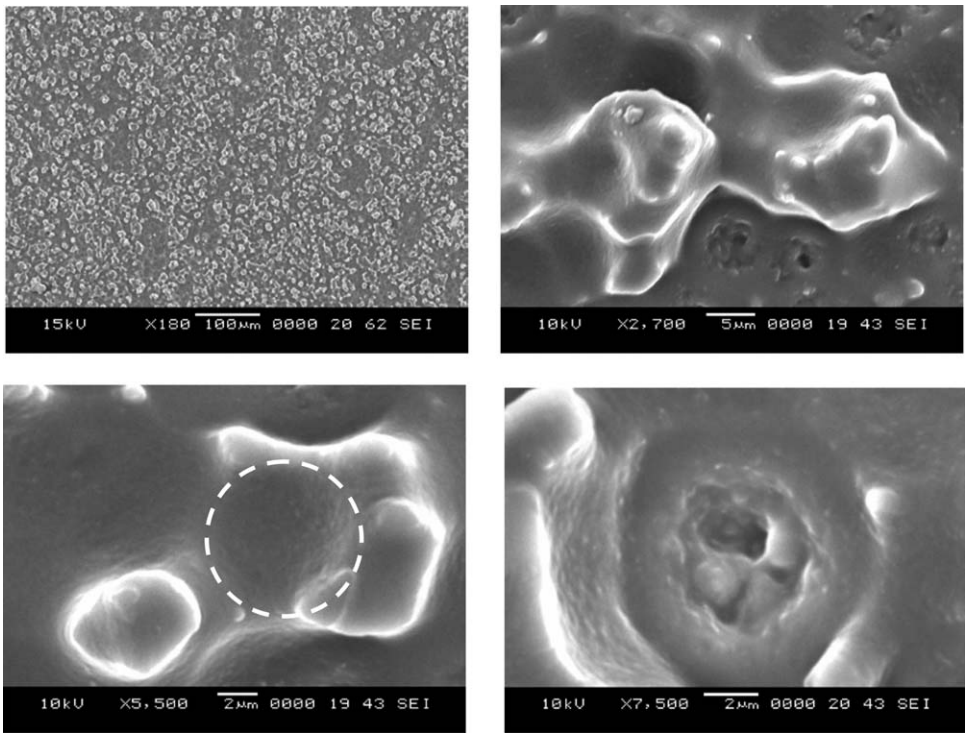

Figure 3. SEM micrographs of the PDMS surfaces after the crystallized PC surfaces were copied after 6 min of immersion: (a) surface copies, (b) copied local texture, (c) copied spherulite without fibrils, and (d) copied spherulite and fibrils.

increased, and nanosize fibrils were initiated from the spherulite surfaces [Figure 2(c)]. As the immersion time progressed further, the spherulites aggregated, and the fibrils covered almost the entire surface [Figure 2(d)] and extended over the spherulite surface [Figure 2(e)] while forming nanotextures. Moreover, the increase in the immersion duration enhanced the coverage area of the fibrils on the spherulite surface. In general, crystals grow radially from potential nucleation sites, and few branches from the nucleation sites occur during radial growth [Figure 2(f)]. Intermittent branching results in the further growth of crystals to form large spherules at the surface, particularly for long immersion durations ($\geq$6 min). The formation of microtextures/nanotextures at the surface is associated with the process of acetone (solvent)-induced crystallization.[22,40–42] Because acetone has Hildebrand solubility parameters on the order of 20.1–20.3 $J^{1/2}/cm^{-3/2}$,[43] it possesses miscible characteristics. Therefore, acetone diffuses into the polymeric structure and forms a swollen film (gelated layer) at the surface during the dissolution. As the diffusion progresses, the glass-transition temperature of the polymeric film behind the diffusion front decreased while causing the plasticization of the swollen polymer.[43] Because the diffusion of acetone into PC was governed by a non-Fickian mechanism,[44,45] the diffusion front between the swollen film and the solid PC penetrated at almost a constant velocity into the solid phase of the amorphous PC.[45,46] Once the PC was removed from the immersion bath, acetone residues at the surface evaporated, and spherulites were initiated to form at PC surface; this was similar to the literature.[47,48] The glass-transition temperature decreased during acetone evaporation from the surface; this, in turn, gave rise to the supercooling of the swollen film and the formation of a surface texture consisting of microsize/nanosize spherulites, cavities, pores, and fibrils. However, the spherulites did not form a well-defined hierarchical structure but instead scattered patterns at the surface [Figure 2(d)]. This behavior could have been related to the nonuniform evaporation of acetone across the entire workpiece surface; it gave rise to various nucleation densities across the surface. However, crystallization occurred in three consecutive phases or categories; these were the crystallization initiation, primary formation of crystals, and secondary crystal growth.[49] A nucleus emerged when the polymer chains gradually aligned in a parallel way, and the chains were added to the nucleus during the initiation of crystallization. Crystal growth became spontaneous after the nucleus size reached the critical size,.[49] The nucleation

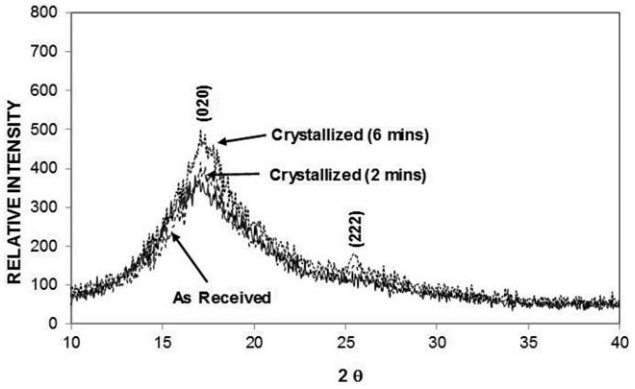

Figure 4. X-ray diffractogram for the crystallized and as-received PC workpieces.

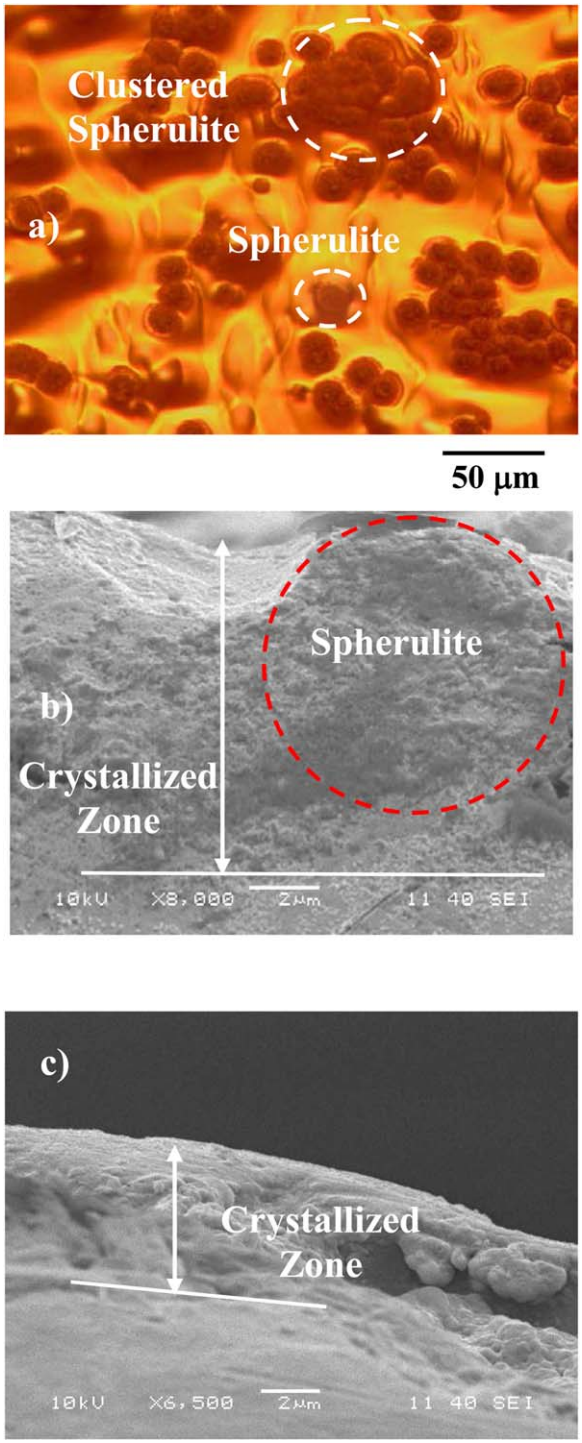

Figure 5. Optical and SEM images of the crystallized PC after 6 min of immersion: (a) optical image of the crystallized surface and spherulites, (b) SEM micrograph of the cross sections of the crystallized layer and spherulite, and (c) SEM micrograph of the cross section of the crystallized layer when no spherulite was formed. [Color figure can be viewed in the online issue, which is available at wileyonlinelibrary.com.]

resulted in bundlelike or lamellar crystallization. The difference between the types of crystallization was associated with size of the primary nucleus and the free energy of the surface normal to the chain direction per unit area.[50] The crystallization mainly started from the molten state of the swollen film. Therefore, the mixture of bundlelike and lamellar nuclei could form because of the series of additions of repeating units during crystallization. Moreover, the presence of small-size cavities and pores resulted in microlevel/nanolevel waviness at the surface and contributed to the overall texture of the crystallized surface. Figure 3 shows SEM micrographs of the PDMS surfaces after removal from the textured PC surface. Because liquid PDMS had excellent rheological properties, it wetted the PC texture feature before solidification. Therefore, it copied almost exactly the texture of the PC surface when it was removed in the solid phase from the PC surface [Figure 3(a)]. These resulted in microsize/nanosize voids and cavities formed at the PDMS surface [Figure 3(b)]. Some fibrils were not clearly observed at the PDMS surfaces [Figure 3(c)]. However, some fibrils on the spherulites were partially copied [Figure 3(d)]. This was attributed to the adhesion between the fibrils and PDMS; this caused broken fibrils during the removal of PDMS. The texture of the spherulite appearance was observed at the PDMS surface. This behavior was attributed to a low E_s of the solid phase of PDMS,[51] which acted like an elastic body during the removal from the textured PC surface. In the case of complex geometric shapes, such as the odd-shaped texture peaks on the PC surface, some residues of the solid phase PDMS remained at the PC surface because of the strong adhesion between the solidified PDMS and the PC surface. Because the PDMS residues left at the PC surface were small, no significant rapturing of the PDMS surface was observed.

Figure 4 shows the XRD of the PC surface with and without immersion in acetone. The immersion durations were kept at 2 and 6 min; this resulted in microtextures/nanotextures composed of spherulites, cavities, pores, and fibrils. The X-ray diffractogram demonstrated that the as-received wafer was totally amorphous; this gave rise to no clear identifiable peak in the diffractogram. The two diffraction peaks were visible in the diffractogram for the crystallized surface. These peaks corresponded to a diffraction angle of 17.1° (020) and 25.7° (222) phases. The peak heights and full width at half-maximum of the peaks differed in the diffractogram. The crystallinity of the textured surface was determined from the ratio of the sum of the integrated intensities of the reflections from the crystalline phases (peaks) to the total scattered intensity after background subtraction.[52] This arrangement resulted in crystallinity values on the order of 36%; these values were higher than those reported in an earlier study.[52] However, the crystallinity of the PC surface depended on the immersion duration, in which case, a longer duration resulted in a high crystallinity at the surface. Therefore, a 2-min immersion duration resulted in a 13% crystallization, and a 6-min immersion duration resulted in a 36% crystallization. Crystal Impact Match 3 software[53] was used to determine the crystallinity. In addition, the optical images were used to account for the spherulites formed on the crystallized PC surface. The typical optical image resulting after 6 min of immersion is shown in Figure 5(a). The findings revealed that the coverage area by the spherulites on the crystallized PC surface was almost 32% of the total surface area. In addition,

Table I. Microhardness and σ Formed in the Crystallized PC Wafers with Different Immersion Durations

		Immersion duration (min)				
Source of variables	As received	2	4	6	8	10
Microhardness (HV)	11.2 ± 0.2	18.1 ± 0.5	22.4 ± 0.9	23.3 ± 0.9	25.2 ± 0.9	25.3 ± 0.9
σ (MPa)	—	—	−26 ± 0.03	−28 ± 0.03	−30 ± 0.03	−30 ± 0.03

Figure 5(b,c) shows the SEM micrograph of the cross section of the crystallized surface. It was evident that the depth of crystallization in the surface region was on the order of a few micrometers. Consequently, the crystallization of the PC surface took place in the surface region. Table I gives the microhardness and residual data obtained for the crystallized PC wafer. Σ was compressive, and it was on the order of −30 MPa. The formation of σ was associated with the high rate of crystallization at the surface during the evaporation of acetone from the surface after removal from the acetone bath. In this case, the modification of molecular structures during crystallization was responsible for stress formation after the immersion process.[54] In addition, the volume change due to hydrolysis affected σ formation in the surface region of PC. However, the stress measurements were carried out immediately after we took the samples from the immersion tank. Figure 6 shows the FTIR data obtained for the crystallized and as-received PC samples. FTIR data for the PDMS samples after the crystallized PC surface was copied are also shown in Figure 6. The as-received sample demonstrated the absorption spectrum of a typical PC wafer.[15] In the case of the crystallized surface, the presence of the absorption band at 2874–2969 cm^{-1} was related to the C—H bond stretching vibrations taking place, and the absorption band at 860–680 cm^{-1} corresponded to the bending vibrations of the C—H bond. The C—H bending vibrations of methylene groups occurred at 1496 cm^{-1}, and aromatic C—H bending vibrations took place at 860–680 cm^{-1}. In addition, the band at 1700–1500 cm^{-1} was related to aromatic C=C bending vibrations, and the C=O stretching vibrations of the ethers occurred at 1770 cm^{-1}. Moreover, we observed that the absorption increased at certain wavelengths for the crystallized surface. This was associated with the crystallinity-induced polymer chains, which were more closely packed. This resulted in the restriction of group vibrations and caused a band intensity increase in the absorption spectrum. Consequently, closely packed polymer chains contributed to σ enhancement, and the microhardness increased in the crystallized PC samples. In the case of the FTIR data for the PDMS sample, two groups of data were observed, namely, silicon–methyl and siloxane groups. A doublet at 1100 and 1020 cm^{-1} corresponded to asymmetric and symmetric stretching vibrations, respectively.[55] The absorption at 800 cm^{-1} was attributed to the out-of-plane oscillation of the Si—CH_3 bonding. The silicon–methyl structural peak occurred at 1250 cm^{-1}.[56] Slight differences in the absorption as compared to that reported in the literature[57] were associated with the solidification rates of liquid PDMS, which made the duration for solidification longer at the PC surface while slightly modifying the absorption characteristics. The depth of the crystallized surface was on the order of a few micrometers, as shown in the SEM micrograph in Figure 5(b,c). Therefore, the absorbance spectra changed in this thin layer compared to that of the as-received PC wafer.

Figure 7 shows the friction coefficients of the crystallized and as-received PC surfaces for different immersion periods. The friction coefficient of the PDMS surfaces, which corresponded to the copy of the textured PC surface, is also included in Figure 7. Crystallization lowered the friction coefficient of the PC surfaces; this was more pronounced for the immersion durations of 6 min or greater. This behavior was attributed to the microhardness enhancement after acetone treatment (Table I). However, the waviness in the friction coefficient was attributed to the surface texture, which consisted of clustered and/or closely spaced spherulites [Figure 5(a)], which demonstrated

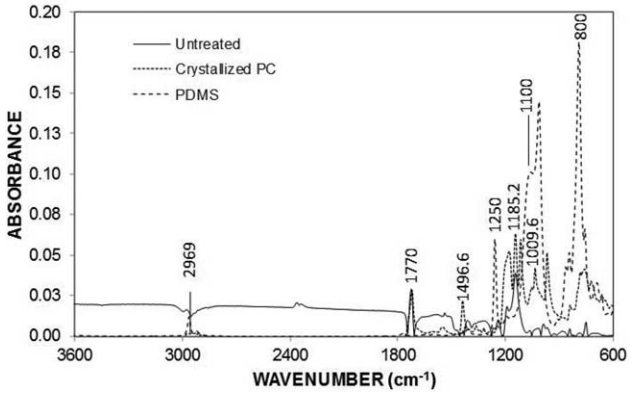

Figure 6. FTIR data for the crystallized and as-received PC samples and copied PDMS.

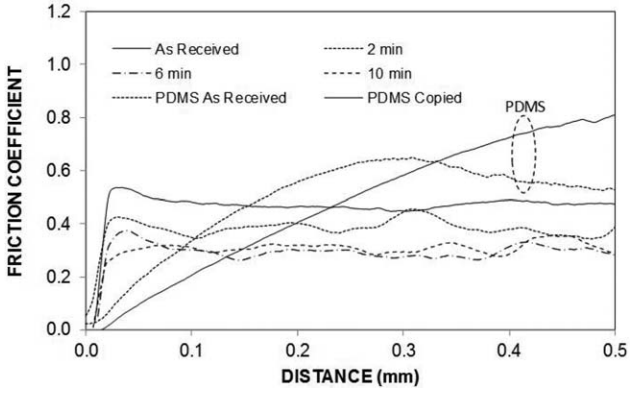

Figure 7. Friction coefficient of the crystallized and as-received PC surfaces for various immersion durations and the copied and as-received PDMS samples.

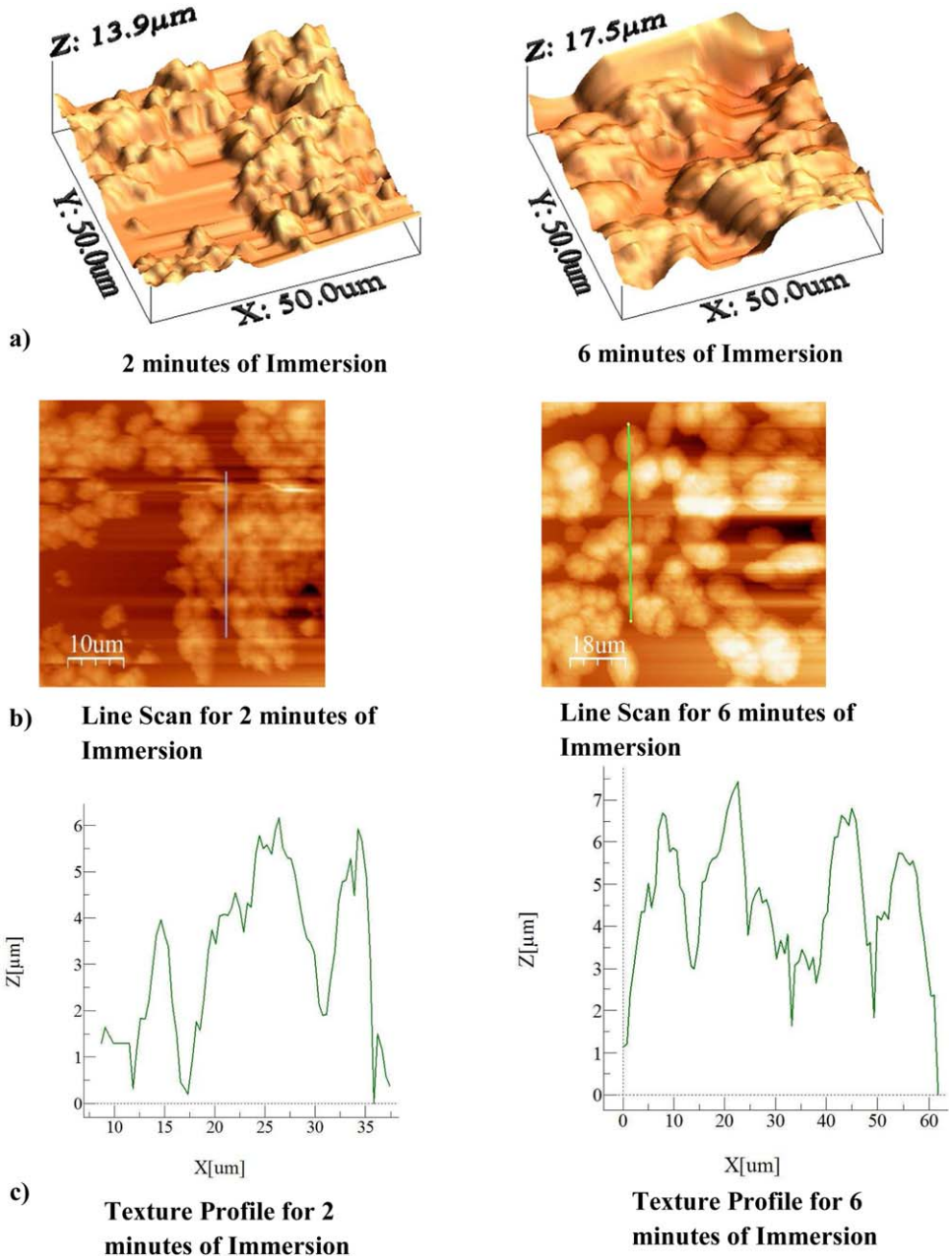

Figure 8. AFM images and texture profile of the crystallized PC surfaces for two immersion durations. Z is the surface texture profile height and X is the distance along the rakes shown in b). [Color figure can be viewed in the online issue, which is available at wileyonlinelibrary.com.]

different hardness configurations because of the plasticizing of the swollen polymer at the surface during crystallization.[44] In addition, the friction coefficient for PDMS was higher than those corresponding to the crystallized PC surface; this was attributed to the small hardness and low E_s of PDMS. The scratch marks left on the PC surface were almost uniform, and the scar size was slightly smaller for the crystallized surfaces than for the as-received surface. However, no microcracks were observed around the scar marks for the crystallized PC surfaces. This revealed that the fracture toughness reduction due to surface hardness enhancement was not significant for the crystallized PC surfaces. Equation (3) was used to determine the H_s values of the crystallized and as-received PC surfaces. The H_s values of the crystallized and as-received PC surfaces were 115 ± 11 and 80 ± 3.2 MPa, respectively. However, the H_s values of the crystallized surface remained almost the same for different immersion times; that is, the variations were within the experimental error (6%). Several tests were conducted on the crystallized surface, and on the basis of the repeatability of the data, the estimated error was on the order of 6%.

To assess the texture characteristics of the crystallized PC surfaces, AFM was used. Figure 8 shows the AFM images of the crystallized PC surfaces and line scans corresponding to two different immersion durations, whereas Figure 9 shows the corresponding AFM images of PDMS. Because the spherulites

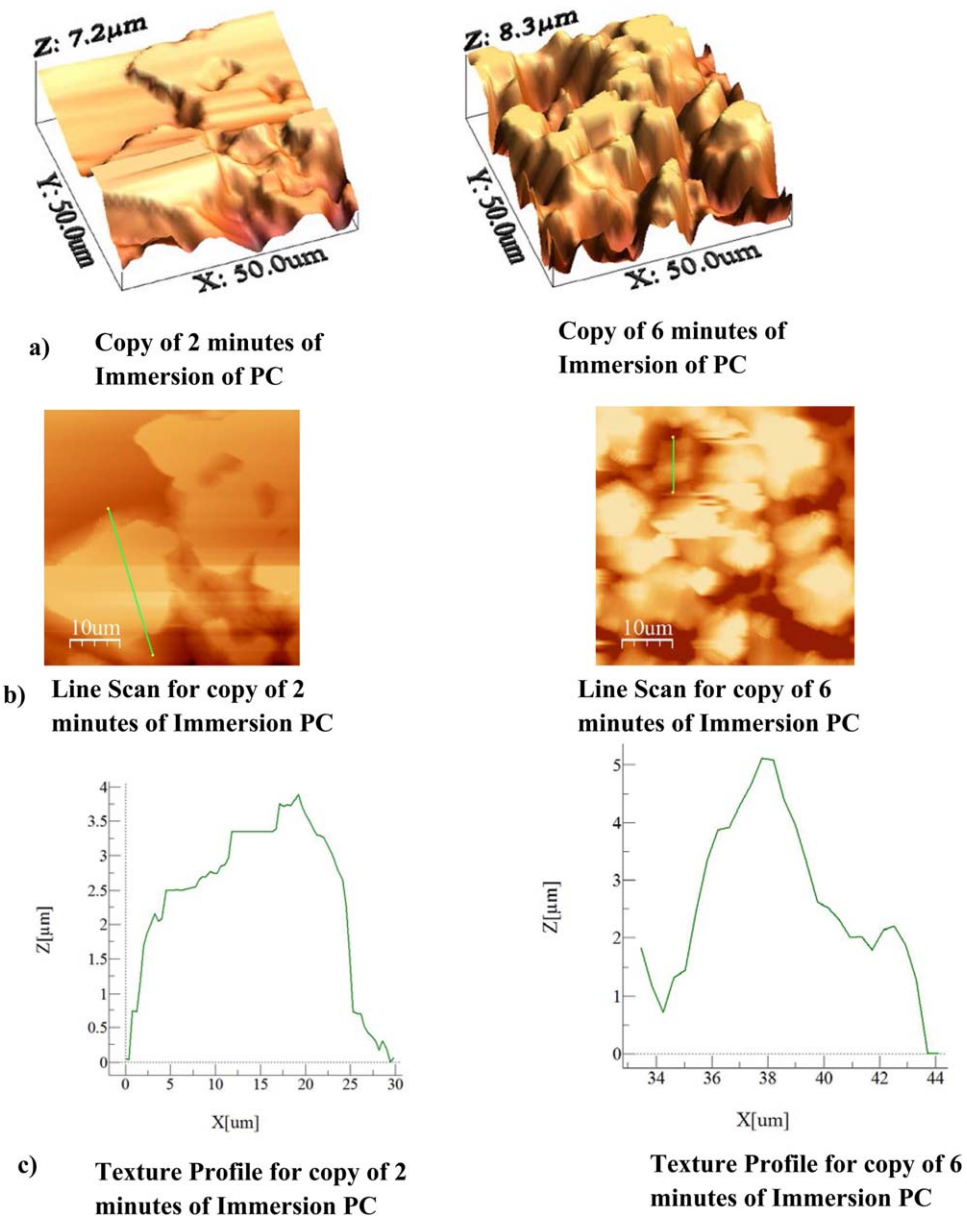

Figure 9. AFM images and texture profile of the EDMS surfaces copied from the PC crystallized surfaces for two immersion durations. [Color figure can be viewed in the online issue, which is available at wileyonlinelibrary.com.]

formed after crystallization did not have exact spherical morphologies at the PC surface, the AFM images showed nonspherical structures at the surface [Figure 8(a)]. However, the height of the nonspherical structures increased slightly, and the coverage area of these structures increased at the surface with increasing immersion time. This behavior was attributed to the rate of formation of nonspherical spherulites at the PC surface with immersion time. In this case, increases in the immersion time enhanced the number of spherulites formed at the PC surface. The surface texture possessed microfibrils/nanofibrils, which formed ripples/waviness in the texture profile, as shown in Figure 8(a,b). Because crystal growth at the PC surface involved multidimensional features, no regular or standard pattern was observed along the texture profiles. The roughness of the crystallized PC surface varied within 3.6–4.3 μm; in this case, an increase in the immersion time increased the roughness of the surface. As shown in Figure 9, in which AFM images of the PDMS surface are shown, the presence of copied nonspherical spherulite-like structures were evident [Figure 9(a)]. Although the crystallized PC was copied, some nanoscale and subnanoscale features were not copied properly from the crystallized PC surface. In this case, the surface texture of PDMS was rather smooth compared to that of the crystallized PC. This situation could also be seen from the texture profile; in this case, ripples/waviness disappeared from the texture profiles of the PDMS surface [Figure 9(b,c)]. Nevertheless, the crystallized PC surface was copied almost exactly at the PDMS surface, except randomly distributed nanosize fibrils and a few voids were not

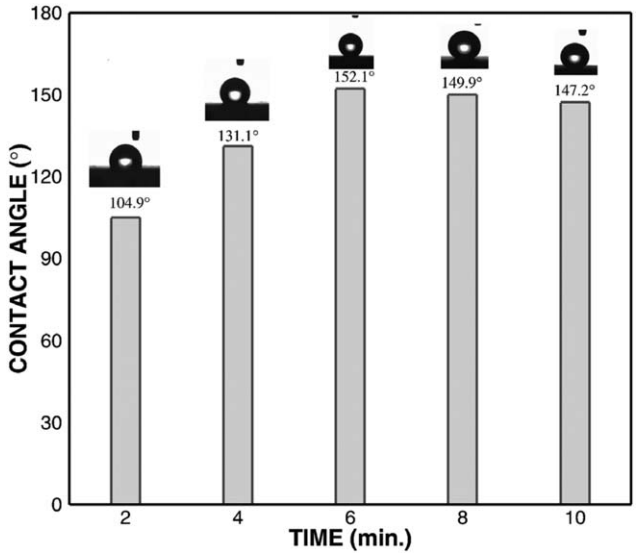

Figure 10. Contact angle variation versus the immersion duration for the crystallized PC.

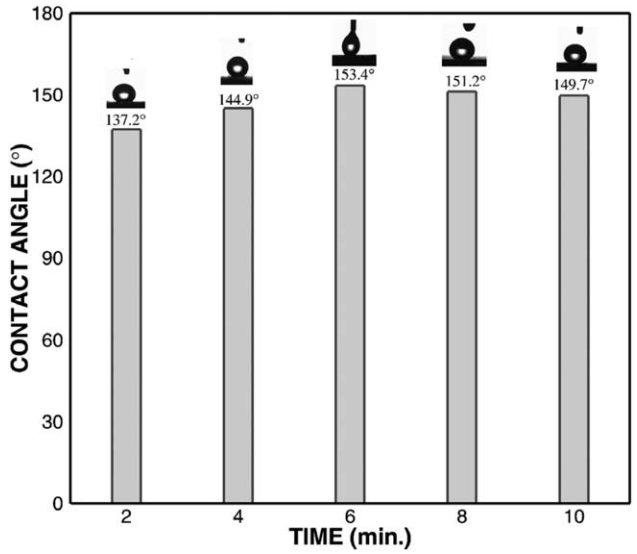

Figure 11. Contact angle variation versus the immersion duration for PDMS after the crystallized PC surface was copied.

copied. This did not notably alter the roughness of the PDMS surface.

Figures 10 and 11 show the distribution of the contact angle and the corresponding images of droplets captured from the sessile contact angle tests for the crystallized PC and copied PDMS surfaces. The main parameters influencing the liquid drop contact angle were the surface free energy of the substrate material and the surface texture. The contact angle of the liquid on the surface was determined by Young's equation.[58] However, the equation is limited to extremely smooth and homogeneous surfaces. On the other hand, the Wenzel and Cassie–Baxter equations for the apparent contact angle (θ_c), which includes the surface roughness, provide more realistic data.[58] When one deals with a heterogeneous surface, the Wenzel model is not sufficient; therefore, a more complex model is needed to determine θ_c for various surfaces with different surface roughnesses.[58] A liquid droplet has liquid–solid and liquid–vapor interfaces, and the contact angle should include contributions of two interfaces. Therefore, the equation for the contact angle yields[58]

$$\cos\ \theta_c = f_1 \cos\ \theta_1 + f_2 \cos\ \theta_2 \quad (4)$$

where f_1 is the surface fraction of the liquid–solid interface, f_2 is the surface fraction of the liquid–vapor interface, θ_1 is the contact angle for the liquid–solid interface, and θ_2 is the contact angle for the liquid–vapor interface. For the air-liquid interface, f_1 can be represented by the solid fraction (f), and the air fraction (f_2) becomes $1 - f$. The parameter f ranges from 0 to 1; in this case, $f = 0$ is the case where the liquid droplet is not in contact with the surface, and $f = 1$ is the case where the surface is completely wetted. However, the contact mode changes from the Cassie–Baxter state to the Wenzel state[59] when the surface texture becomes sparse or when the droplets impact the surface with a high velocity.[60] The crystallized PC surface had the texture feature, and this resulted in the Cassie–Baxter state. Consequently, the surface texture with a combination of microspherulites/nanospherulites, voids, and fibrils gives rise to air pockets being trapped in the texture and result in the Cassie–Baxter state in the crystallized PC and copied PDMS surfaces. Because the surface free energy was lower for PDMS (19.8 mN/m)[57] than for PC (34.2 mN/m),[61] the contact angle remained slightly higher for the copied PDMS surface. In addition, small differences between the contact angles, because of

Table II. Contact Angle Measurement for the Crystallized PC Surface and the Copied PMDS Surface

			Immersion duration (min)				
Source of variables		As received	2	4	6	8	10
PC	Advancing	82	104	151	152	150	147
	Receding	56	98	147	148	145	143
	Hysteresis	26	6	4	4	5	4
PDMS	Advancing	104	137	145	153	151	149
	Receding	97	131	137	146	145	142
	Hysteresis	7	6	8	7	6	7

The measurement errors was between 4° and −4°.

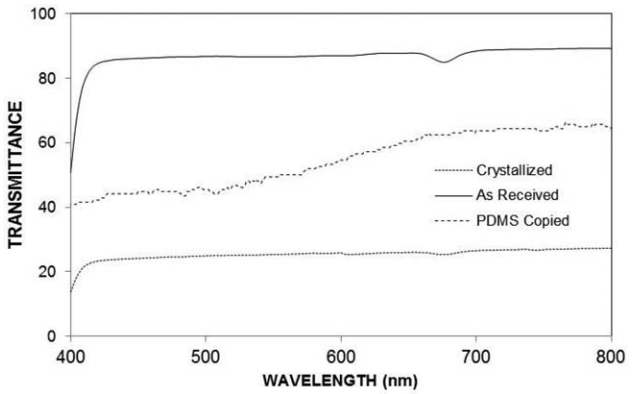

Figure 12. Transmittance data for the as-received and crystallized PC after 6 min of immersion and the PDMS sample after the copied PC surface was immersed for 6 min in acetone.

the crystallized PC and replica PDMS surface, were associated with the surface texture differences between the two surfaces. In this case, nanosize and subnanosize fibrils and voids were not copied exactly by PDMS from the crystallized PC surface. Therefore, despite the large difference in the surface free energy of both samples, the surface texture difference in detail suppressed the contact angle difference corresponding to both surfaces. Table II gives the hysteresis angles ($\theta_{\text{Hysteresis}} = \theta_{\text{Advancing}} - \theta_{\text{Receding}}$, where $\theta_{\text{Advancing}}$ is the advancing angle and θ_{Receding} is the receding angle) of the crystallized and copied PDMS surfaces. The hysteresis corresponding to the copied PDMS surface was slightly higher than that of the hysteresis corresponding to the crystallized PC surfaces. This was attributed to the nonpresence of nanosize and subnanosize fibrils; this was responsible for the increased hysteresis of the copied PDMS surface. Figure 12 shows the optical transmittance of the crystallized PC wafers and their copy of PDMS with 6 min of immersion. The transmittance data for the as-received PC and PDMS are also included for the comparison reasons. The crystallization of the PC surface significantly reduced the transmittance; in this case, the increase in the immersion time lowered the transmittance of the crystallized PC wafer. In the case of the copied PDMS, the transmittance remained higher than that of the crystallized PC; however, the transmittance decreased almost 40% compared to the original PDMS transmittance. This was attributed to the scattering of incident radiation from the sample surfaces because of the textures developed after the copying of the crystallized PC surface.

CONCLUSIONS

The surface texturing of PC wafers by immersion in acetone and the copying of the textured surface by PDMS were carried out. The influence of the immersion duration on the surface crystallization of the PC wafers was examined. The morphological, hydrophobic, and tribological characteristics of the crystallized surfaces and their copies were investigated with analytical tools, including SEM, AFM, XRD, FTIR spectroscopy, UV–vis spectroscopy, sessile drop measurement, and microtribometry. The PC surfaces were crystallized in liquid acetone with the immersion technique. Liquid PDMS was used to copy the texture of the crystallized PC surface. We found that the crystallized PC surface consisted of microsize/nanosize spherulites, voids, and fibrils. Increases in the immersion duration enhanced the texture height and concentration of spherulites and fibrils formed at the PC surface. The surface texture demonstrated the nonhierarchical distribution of spherulites; in addition, the line profile of the surface demonstrated the presence of nanosize ripples/wavy structures at the surface of the spherulites. The roughness of the crystallized PC surface changed with immersion duration; in this case, increases in the immersion duration gave rise to roughness enhancement at the PC surface. Σ formed in the PC wafer was compressive, and it was on the order of -30 MPa. The H_s of the crystallized PC surfaces was 115 ± 11 MPa, and it remained almost the same for all immersion durations. The PDMS surface texture was almost an exact copy of the crystallized PC surface, except for the nanosize and subnanosize fibrils, which were not captured. The friction coefficient of the crystallized surface was lower than that of the as-received PC surface, and increases in the immersion time lowered the friction coefficient because of the microhardness increase after crystallization. The surface hydrophobicity significantly improved for the crystallized PC, and the maximum contact angle achieved was on the order of 152°, which corresponded to 6 min of immersion. The PDMS copying of the crystallized surface texture resulted in a higher contact angle than those of the crystallized PC surfaces. This was attributed to the low surface energy of PDMS, even though nanosize and subnanosize fibrils were not copied by PDMS. The optical transmittance of the crystallized PC wafer was reduced significantly because of the absorption and scattering of incident radiation by the surface texture; however, the optical transmittance remained reasonably high for the PDMS samples.

ACKNOWLEDGMENTS

The authors acknowledge the financial support of King Fahd University of Petroleum and Minerals and King Abdulaziz City for Science and Technology through contract grant number 11-ADV2134-04 to complete this study.

REFERENCES

1. Wagner, T.; Neinhuis, C.; Barthlott, W. *Acta Zool.* **1996**, *77*, 213.
2. Parker, A. R.; Lawrence, C. R. *Nature* **2001**, *414*, 33.
3. Gao, X.; Jiang, L. *Nature* **2004**, *432*, 36.
4. Byun, D.; Hong, J.; Saputra, Ko, J. H.; Lee, Y. J.; Park, H. C.; Byun, B. K.; Lukes, J. R. *J. Bionic Eng.* **2009**, *6*, 63.
5. Koch, K.; Bhushan, B.; Barthlott, W. *Soft Matter* **2008**, *4*, 1943.
6. Azimi, G.; Dhiman, R.; Kwon, H.-M.; Paxson, A. T., Varanasi, K. K. *Nat. Mater.* **2013**, *12*, 315.
7. Han, J. T.; Xu, X. R.; Cho, K. W. *Langmuir* **2005**, *21*, 6662.
8. Shirtcliffe, N. J.; McHale, G.; Newton, M. I.; Chabrol, G.; Perry, C. C. *Adv. Mater.* **2004**, *16*, 1929.

9. Hwang, H. S.; Lee, S. B.; Park, I. *Mater. Lett.* **2010**, *64*, 2159.
10. Huang, Y. H.; Wu, J. T.; Yang, S. Y. *Microelectron. Eng.* **2011**, *88*, 849.
11. Yang, T.; Tian, H.; Chen, Y. *J. Sol–Gel Sci. Technol.* **2009**, *49*, 243.
12. Kinoshita, H.; Ogasahara, A.; Fukuda, Y.; Ohmae, N. *Carbon* **2010**, *48*, 4403.
13. Latthe, S. S.; Imai, H.; Ganesan, V.; Rao, A. V. *Appl. Surf. Sci.* **2009**, *256*, 217.
14. Ma, M.; Mao, Y.; Gupta, M.; Gleason, K. K.; Rutledge, G. C. *Macromolecules* **2005**, *38*, 9742.
15. Yilbas, B. S.; Khaled, M.; Abu-Dheir, N.; Al-Aqeeli, N.; Said, S. A. M.; Ahmed, A. O. M.; Varanasi, K. K.; Toumi, Y. K. *Appl. Surf. Sci.* **2014**, *320*, 21.
16. Zhang, X.; Guo, Y.; Zhang, P.; Wu, Z.; Zhang, Z. *Mater. Lett.* **2010**, *64*, 1200.
17. El Ghanem, H. M.; Saqa'n, S. A.; Al-Saadi, M.; Abdul Jawad, S. M. *J. Mod. Phys.* **2011**, *2*, 1553.
18. Grebowicz, J. S. *J. Therm. Anal.* **1996**, *46*, 1151.
19. Sung, Y. T.; Fasulo, P. D.; Rodgers, W. R.; Yoo, Y. T.; Yoo, Y.; Paul, D. R. *J. Appl. Polym. Sci.* **2012**, *124*, 1020.
20. Lee, C.-H.; Katoa, M.; Usukia, A. *J. Mater. Chem.* **2011**, *21*, 6844.
21. Madsen, M. H.; Feidenhans'l, N. A.; Hansen, P. E.; Garnæs, J.; Dirscher, K. *J. Micromech. Microeng.* **2014**, *24*, 127002.
22. Cui, Y.; Paxson, A. T.; Smyth, K. M.; Varanasi, K. K. *Colloids Surf. A* **2012**, *394*, 8.
23. Jang, M.; Park, C. K.; Lee, N. Y. *Sens. Actuators B* **2014**, *193*, 599.
24. Soliveri, G.; Sabatini, V.; Farina, H.; Ortenzi, M. A.; Meroni, D.; Colombo, A. *Colloids Surf. A* **2015**, *483*, 285.
25. Jiang, M.; Liu, J. G.; Wang, S. H.; Lv, M.; Zeng, X. Y. *Surf. Coat. Technol.* **2014**, *254*, 423.
26. Zhou, Y.; Dan, Y.; Jiang, L.; Li, G. *Polym. Degrad. Stab.* **2013**, *98*, 1465.
27. Bhagat, S. D.; Gupta, M. C. *Surf. Coat. Technol.* **2015**, *270*, 117.
28. Bormashenko, E.; Chaniel, G.; Gendelman, O. *J. Colloid Interface Sci.* **2014**, *435*, 192.
29. Saarikoski, I.; Suvanto, M.; Pakkanen, T. A. *Appl. Surf. Sci.* **2009**, *255*, 9000.
30. Yu, D.; Zhao, Y.; Li, H.; Qi, H.; Li, B.; Yuan, X. *Prog. Org. Coat.* **2013**, *76*, 1435.
31. Soz, C. K.; Yilgor, E.; Yilgor, I. *Polymer* **2015**, *62*, 118.
32. Goel, P.; Kumar, S.; Kapoor, R.; Singh, J. P. *Appl. Surf. Sci.* **2015**, *356*, 102.
33. Juarez-Moreno, J. A.; Ávila-Ortega, A.; Oliva, A. I.; Aviles, F.; Cauich-Rodriguez, J. V. *Appl. Surf. Sci.* **2015**, *349*, 763.
34. Liu, X.; Xu, Y.; Ben, K.; Chen, Z.; Wang, Y.; Guan, Z. *Appl. Surf. Sci.* **2015**, *339*, 94.
35. Tompkins, B. D.; Fisher, E. R. *J. Appl. Polym. Sci.* **2015**, *132*, 41978.
36. Zhang, L.; Yu, H.; Zhao, N.; Dang, Z.-M.; Xu, J. *J. Appl. Polym. Sci.* **2014**, *131*, 41057.
37. Gilliam, M.; Yu, Q. *J. Appl. Polym. Sci.* **2007**, *105*, 360.
38. Totemeier, T. C.; Wright, R. N. *Surf. Coat. Technol.* **2006**, *200*, 3995.
39. Standard Test Method for Evaluation of Scratch Resistance of Polymeric Coatings and Plastics Using an Instrumented Scratch Machine; ASTM D 7027-05; ASTM International: West Conshohocken, PA, **2005**. http://www.astm.org/DATABASE.CART/HISTORICAL/D7027-05.htm.
40. Turska, E.; Benecki, W. *J. Appl. Polym. Sci.* **1979**, *23*, 3489.
41. Durning, C. J.; Rebenfeld, L.; Russel, W. B.; Weigmann, H. D. *J. Polym. Sci. Part B: Polym. Phys.* **1986**, *24*, 1321.
42. Im, S. H.; Herricks, T.; Lee, Y. T.; Xia, Y. *Chem. Phys. Lett.* **2005**, *401*, 19.
43. Grulke, E. A.; Brandrup, J.; Immergut, E. H. Polymer Handbook; Wiley: New York, **1999**.
44. Van Krevelen, D. W. Properties of Polymers: Their Correlation with Chemical Structure; Elsevier: Amsterdam, **1972**.
45. Alfrey, T.; Gurnee, E. F.; Lloyd, W. G. *J. Polym. Sci. Part C: Polym. Lett.* **1966**; Vol. *12*, p 249.
46. Sanopoulou, M.; Stamatialis, D. F. *Polymer* **2001**, *42*, 1429.
47. Dayal, P.; Guenthner, A. J.; Kyu, T. *J. Polym. Sci. B: Polym. Phys.* **2007**, *45*, 429.
48. Pekarek, K. J.; Jacob, J. S.; Mathiowitz, E. *Adv. Mater.* **1994**, *6*, 684.
49. Lauritzen, J., Jr.; Hoffman, J. D. *J. Res. Natl. Bur. Stand. Sect. A* **1960**, *64*, 73.
50. Frank, F. C.; Tosi, M. *Proc. R. Soc. (London) Ser. A* **1961**, *263*, 323.
51. Schneider, F.; Draheim, J.; Kamberger, R.; Wallrabe, U. *Sens. Actuators A* **2009**, *151*, 95.
52. Fan, Z.; Shu, C.; Yu, Y.; Zaporojtchenko, V.; Faupel, F. *Polym. Eng. Sci.* **2006**, *46*, 729.
53. Crystal Impact. MATCH! Phase Identification from Powder Diffraction. **2015**, http://www.crystalimpact.com/match/.
54. Li, L.; Shi, L.; Chen, Y.; Zhang, Y.; Guo, Z.; Su, B.; Liu, W. *J. Mater. Chem. A* **2012**, *22*, 9774.
55. Aguiar, K. R.; Santos, V. G.; Eberlin, M. N.; Rischka, K.; Noeske, M.; Tremiliosi-Filho, G.; Rodrigues-Filho, U. P. *R. Soc. Chem. RSC Adv.* **2014**, *4*, 24334.
56. Smith, A. L. Chemical Analysis; Wiley: New York, **1991**; Vol. *112*, p 320.
57. Gaboury, S. R.; Urban, M. W. *Polym. Commun.* **1991**, *32*, 390.
58. Jung, Y. C.; Bhushan, B. *Scr. Mater.* **2007**, *57*, 1057.
59. Wenzel, R. N. *Ind. Eng. Chem.* **1936**, *28*, 988.
60. Deng, T.; Varanasi, K.; Hsu, M.; Bhate, N.; Keimel, C.; Stein, J.; Blohm, M. *Appl. Phys. Lett.* **2009**, *94*, 133109.
61. Solid Surface Energy Data (SFE) for Common Polymers. http://www.surface-tension.de/solid-surface-energy.htm.